Available online at www.sciencedirect.com
ScienceDirect
Journal of Nuclear Materials 362 (2007) 274–282
journal of nuclear materials
www.elsevier.com/locate/jnucmat

Local atomic structure in iron copper binary alloys: An extended X-ray absorption fine structure study

G. Kuri [a,*], C. Degueldre [a], J. Bertsch [a], J. Rothe [b]

[a] LWV, NES, Paul Scherrer Institute, 5232 Villigen PSI, Switzerland
[b] INE, Forschungszentrum Karlsruhe, 76344 Karlsruhe, Germany

Abstract

Understanding the clustering process and the evolution of the precipitate structure of copper in Fe–Cu system is an important step in the description of material hardening and the embrittlement process normally observed under irradiation conditions. In this work, an extended X-ray absorption fine structure (EXAFS) spectroscopy characterization of Fe–0.3 wt%Cu and Fe–1.0 wt%Cu binary model alloys has been performed in order to investigate the local structure around Cu and Fe atoms in the matrix. The effect of thermal ageing was studied on one Fe–Cu specimen containing 1.0 wt% Cu annealed at 775 K for a duration of 1 h. The near-neighbour environment of Cu and Fe was examined by determining the best-fit structural parameters after curve fitting to the first-few-shells EXAFS functions. The results provide an indication of the formation of sub-nanometer-size Cu clusters in Fe matrix for the specimens examined. The average structural parameters estimated from the EXAFS data are presented and discussed.

PACS: 61.10.Ht; 61.46.Bc; 61.66.Dk

1. Introduction

Precipitation of copper in iron and steels draws a considerable attention due to its potential effect on material hardening as well as embrittlement processes, particularly in reference to reactor pressure vessel (RPV) steels which are components in nuclear reactors [1,2]. The strength of such Fe_xCu_{100-x} (subscript in at.% unless otherwise specified) composites with varying Cu content is derived from both solid-solution strengthening and precipitation strengthening. During operation the RPV of light water reactors is subjected to factors which lead to ageing of the ferritic steel structures where precipitates are the dominant embrittling feature. Apart from high temperature and high pressure influences, neutron irradiation is another main reason for the material degradation. It is furthermore believed that the irradiation hardening and related embrittlement of RPV steels are very sensitive to the amount of residual copper [3]. Therefore, the formation and/or dissolution of Cu precipitates in Fe–Cu system have been extensively studied, both theoretically and experimentally, over the last years [4–8]. A variety of experimental techniques such as transmission electron microscopy [9,10], field ion microscopy

* Corresponding author. Tel.: +41 56 310 2182; fax: +41 56 310 2203.
E-mail address: goutam.kuri@psi.ch (G. Kuri).

0022-3115/$ - see front matter © 2007 Elsevier B.V. All rights reserved.
doi:10.1016/j.jnucmat.2007.01.275

[11], atom-probe topography [12], etc. has been used for understanding the clustering and precipitation behaviour in this material. Some work has also concentrated on the solid solubility and microstructure of Fe_xCu_{100-x} with a higher Cu concentration above 10 at.%. On the basis of the results of these studies it is generally accepted that *bcc* solid solutions are formed on the Fe-rich side for $x > 80$ and single phase *fcc* solid solutions are obtained for $x < 60$. For the range spanning approximately $60 < x < 80$, a two phase region with coexisting *bcc* and *fcc* solution phases can be expected. However, the mechanism responsible for significantly enhanced solubility and the presence of an obvious two phase coexistence region are still a subject of debate [13].

To the best of our knowledge, the microstructural aspect of Fe–Cu alloy containing very low amount of Cu near its solubility limit is less well characterized in this regard. Cu is practically immiscible in Fe at room temperature. Its solubility at the typical ageing temperatures (i.e., ~775 K or so) is known to be very low (⩽0.1 at.% [11,14]) so that even for typical RPVs with Cu, an impurity present in a saturated solid-solution phase, can provoke significant effects [3]. Recently, employing 3D atom-probe technique, Pareige et al. [15] have measured the mean size and number density of irradiation induced heterogeneous copper clusters in binary Fe–Cu (0.088 at.% Cu) specimens. However, the study is limited to the case for MeV electrons and keV ions irradiated conditions. Since the atomic radii of Cu and Fe are nearly equal and mixing volumes are of the order of 3% due to atomic size mismatch [16], the composition uniformity or the near-neighbour atomic environment in the matrix is nearly impossible to measure by conventional experimental techniques mentioned above. X-ray absorption spectroscopy (XAS) technique, such as extended X-ray absorption fine structure (EXAFS) and X-ray absorption near edge structure (XANES), is a very powerful tool in this field because of the advantages of its atomic selectivity and nondestructive method. It will be shown in the paper that such a technique related to synchrotron radiation is more appropriate. Information can be obtained on the atomic arrangement of nanometer scale metallic particles. In Table 1 several analytical techniques are compared for their performance/detection limits in terms of size and the order of magnitude of the clusters/precipitates that can be detected. EXAFS has been previously used to investigate local atomic environment of Cu and Fe in Fe_xCu_{100-x} ($x \leqslant 90$) system [13,17] and binary Fe–1.3 wt%Cu model alloy [18]. A Cu concentration of about 1.5 wt% has been, however, a limit for the XAS studies [19]. The recent development of high intensity synchrotron radiation sources now allows these studies to be extended to low concentrations of absorbing element, e.g. Cu in the present case, by using fluorescence detection techniques and multi-element solid-state detectors. In this work, employing XAS method, it is aimed at studying the local structure around Cu and Fe atoms in two Fe–Cu binary model alloy samples with different Cu content in the range of 0.3–1.0 wt%. The effect of thermal ageing was studied on one Fe–Cu specimen containing 1.0 wt% Cu annealed at 775 K for a duration of 1 h. The near-neighbour environment of Fe and Cu are examined by analyzing XANES spectra and by determining the best-fit structural parameters after curve fitting to the first-few-shells EXAFS functions.

Table 1
Comparison among several experimental techniques for their performance/detection limits in analyzing clusters and/or precipitates

Experimental methods	Size (nm)	Precipitates density (cm^{-3})
Transmission electron microscopy	~1	$\sim 10^{13}$
Positron annihilation spectroscopy	~0.6	$\sim 10^{14}$
Small angle neutron scattering	~1.2	$\sim 10^{15}$
Atom probe topography	~0.5	$\sim 10^{13}$
Extended X-ray absorption fine structure	0.2–0.8	$\sim 10^{15}$

2. Experimental and data analysis

The specimens used in this investigation were prepared at SCK-CEN, Mol Belgium. Commercial ultrapure elemental powders of Cu (purity 6 N wt%) and Fe (purity 5 N wt%) were used as starting materials. After alloying to the desired compositions, they were preannealed for 4 h under argon ambient at 1075 ± 5 K and quench cooled in water from the annealing temperature. Two samples of the alloys (Fe–0.3 wt%Cu and Fe–1.0 wt%Cu) with a surface polished to an optical quality, were studied using XAS. Apart from these as-prepared specimens, another piece of Fe–1.0 wt%Cu isothermally aged at 775 ± 5 K for 1 h and quenched to room temperature in oil after the ageing treatment, was also selected for XAS investigation.

Fluorescence yield detection is a good method to measure the EXAFS signal because it is very sensitive for samples with small quantity of matter and because the probing depth is large enough to be sure that the bulk structure is sounded. Fluorescence spectra were obtained with a geometry where the fluorescence detector forms an angle of 90° with the incoming beam. The X-ray absorption spectra at the Fe K-edge were recorded using radiation at the Swiss Light Source (SLS) on beam line μ-XAS (X05LA). The beam line is currently equipped with a single-element Si-detector (manufacturer: KETEK GmbH, Germany) for fluorescence measurements. The Cu K-edge spectra were obtained from INE beamline at the ANKA synchrotron radiation laboratory, Forschungszentrum Karlsruhe. The incident X-ray intensities were measured by means of a nitrogen filled ionization chamber. Samples were held at room temperature and the fluorescence excitation spectra were recorded with a 5-element solid-state Ge detector array cooled at 77 K. Each channel of each scan was examined for glitches prior to averaging. Data were also collected from high purity iron and copper metallic foils for use as structural comparators and reference spectra. Energy output of the double-crystal Bragg monochromator was calibrated with the foils with edge energies 7111.9 and 8979.0 eV for Fe and Cu, respectively, set equal to the maximum of the first derivative of the XANES data.

EXAFS data processing and analysis were performed using the University of Washington-Naval Research Laboratory 'FEFFIT' analysis program [20]. Considering the measurements geometry, an appropriate correction has been applied to all the experimental data for the self-absorption effect [20]. The background in the pre-edge and post-edge regions were removed by simulating the data by a cubic spline function. Thus, background-removed EXAFS function $\chi(k)$ was extracted and normalized by the edge jump height. $\chi(k)$ was then multiplied by k^3 to emphasize the higher k region. Thereafter, k^3-weighted EXAFS was Fourier transformed into real space to obtain a radial distribution function (RDF). The first shell EXAFS contributions, corresponding to the nearest copper or iron atoms, were exclusively singled out by the Fourier filtering. Transform termination effects were minimized by choosing the transformation region as bounded by minima in $|\chi(k)|$ and using a Hanning window function that smoothed the ends of the region to zero.

In the next step, the extracted experimental EXAFS signals were best-fitted to the well known EXAFS equation [21]:

$$\chi(k) = \sum_j S_0^2 (N_j/kR_j^2) F_j(k) \exp(-2\sigma_j^2 k^2) \times \exp(-2R_j/\lambda_j(k)) \sin(2kR_j + \phi_j(k)), \quad (1)$$

$$k = \hbar^{-1}[2m_e(E - E_0)]^{1/2}, \quad (2)$$

where S_0^2 is the amplitude reduction factor due to many-electron effects, $\lambda_j(k)$ is the electron mean free path; the sum is over the j coordination shell having N_j atoms put at an average distance R_j from the absorbing atom. $F_j(k)$ is the atomic backscattering amplitude, ϕ_j the phase shift of the jth coordination shell, and σ_j^2 the corresponding Debye–Waller (DW) factor. k represents the magnitude of the photoelectron wavevector and is related to the X-ray energy by Eq. (2). E denotes the energy of the incident X-ray photons and E_0 is the threshold energy for the removal of the core electron.

The set of optimized structural parameters derived from the fits were R_j, N_j, σ_j^2 and ΔE_0 (a correction to E_0). The degree of mismatch between the fitted theoretical standard and the data is given by the EXAFS $\Re$-factor, a standard measure of the quality of the fit. The backscattering amplitude and phase shift functions, required in the calculation of the EXAFS signals in Eq. (1), were obtained from the real space multiple-scattering theory and modern relativistic code FEFF [22]. This code has a number of attractive properties. For example, one can calculate an absorption spectrum in the XANES as well as EXAFS ranges by considering a small cluster of atoms centered on the absorbing atom in each material without any assumption of periodicity or symmetry, which is a major interest of the present work.

3. Results and discussion

The XAS spectrum and associated Fourier transform (FT) obtained for Fe from the 1.0 wt% Cu specimen is shown in Fig. 1. The XANES spectrum and the derivative of the same data are also depicted in Fig. 1(a) as insets. The iron spectra from 0.3 wt % Cu alloy and 775 K annealed specimen are similar and hence not presented here. The edge position, taken as the maximum of the first derivative of the spectrum, reveals an E_0 value of 7111.93 eV which is indeed identical to the reference K-edge excitation energy of iron metal (7111.99 eV). This information

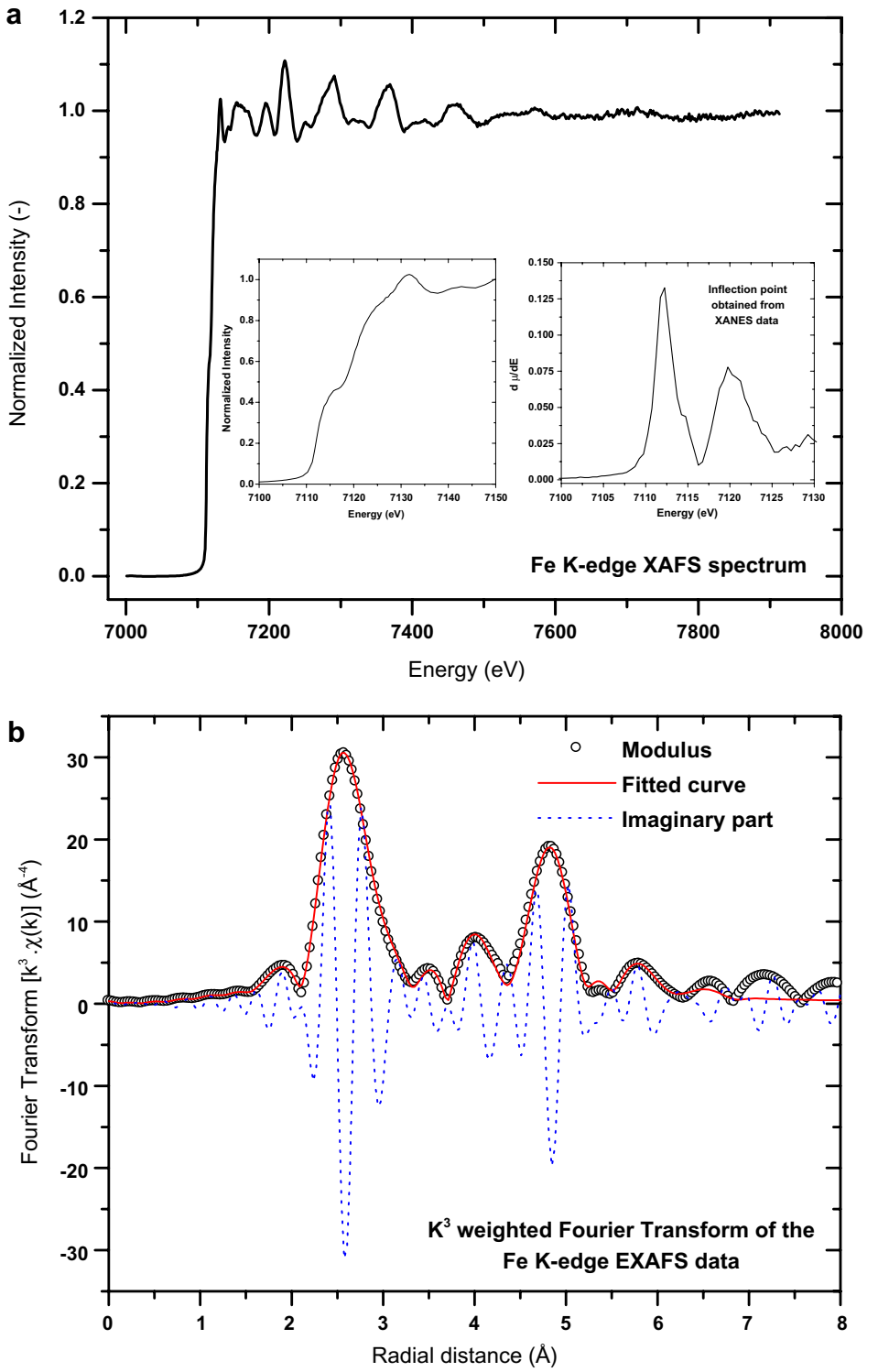

Fig. 1. (a) Fe K-edge absorption spectrum of Fe–1.0 wt%Cu specimen in the as-prepared state. In the inset XANES spectrum and the first derivative of XANES data are shown. (b) Magnitude of the k^3 weighted Fourier transformed EXAFS signal (dot line), imaginary part of the transform (dash line) and best-fitted curve (solid line) are shown.

can be used to determine if the spectral shape and the electronic states of Fe in the specimens are altered in response to any chemical extractants, e.g. Cu atoms in the present case. However, this is not observed. The reason for this may be due to the fact that the high-density Fe d states are poorly matched in energy with low-density Cu s states. As a result, the addition of Cu is not expected to influence significantly the electronic structure of Fe near the Fermi surface [23], at least until a significant amount of copper is present.

For a quantitative analysis of the data in Fig. 1(a), the fitting procedure on the EXAFS signal and on its FT was adopted using the standard methods as summarized above. This was necessary to obtain the structural parameters of Fe to compare with that of an iron metallic foil and for using them in analyzing the Cu data. This point will be discussed later in this section. The analyzed FT result for Fe is depicted in Fig. 1(b). The analysis using FEFF model of the *bcc* Fe crystal lattice structure yielded a very good fit to the experimental data. The FEFF model comprises all single scattering paths from various shells and all multiple-scattering paths up to 0.6 nm. The Fe atom is surrounded by 8 atoms at 0.249 nm, 6 at 0.287 nm, 12 at 0.406 nm, 24 at 0.476 nm and 8 at 0.497 nm in the first five consecutive neighbour shells. The data in Fig. 1(b) have been corrected for electron phase shifts using the first shell-path from FEFF and therefore, the FT peaks should correspond directly with the true bond distances of the near neighbours. Results of the first coordination shell fitting parameters obtained are: an Fe–Fe coordination number of 7.9 ± 0.3 at a distance 0.248 ± 0.002 nm, $\sigma^2 = (41 \pm 5) \times 10^{-4}$ Å^2 and $\Delta E_0 = 7.16$ eV; whereas the corresponding values for the second shell are $N = 6.2 \pm 0.2$, $R = 0.285 \pm 0.002$ nm, $\sigma^2 = (48 \pm 5) \times 10^{-4}$ Å^2 and $\Delta E_0 = 7.16$ eV; in agreement with the parameters known in the literature [24]. The estimated errors are the standard ones for EXAFS. These data clearly show a representation of *bcc* unit cell for the used Fe substrate. In fact, from the data measured at the Fe K-edge and their analyses, any difference was not observed between an Fe-foil and the Fe–Cu specimens. However, this is not the case for that of the Cu absorber.

In the next, let us consider the data measured at the Cu K-edge. In Fig. 2(a) the XAS spectra are shown both for the binary Fe–Cu samples and for the reference Cu foil. All Cu data were converted to k-space using $E_0 = 8979$ eV. These curves, weighted by k^3 have been Fourier transformed and fit using 'FEFFIT' algorithm. The results are also shown in Fig. 2(b) and best-fit values of the structural parameters are included in Table 2. Data collected from Cu and Fe foils were similarly analyzed after correcting for self-absorption effect and presented in Fig. 2 as a standard of the *fcc* and *bcc* structures, respectively. In this way, the data can be compared in terms of amplitude and phases of the EXAFS oscillations to determine similarities or differences among specimens, between samples and foils, and also to provide information as to the signal-to-noise characteristics of the experiment.

From the XAS spectra as well as RDFs in Fig. 2, it is clear that the Cu spectra of three alloy samples can be well described by the Cu *bcc* model as in the Fe metal foil. The Cu-foil spectrum presented in Fig. 2(b) illustrates Fourier features which are characteristics of the *fcc* sites environments and the shape of RDF is quite different from that of the Fe-foil and/or the Fe–Cu specimens. The RDF of Fe K-edge for the metal foil shows that there are three strong amplitude peaks between 0.2 and 0.5 nm whose distance R is around 0.25, 0.37 and 0.47 nm, respectively. The first strong peak at 0.25 nm stems from first and second neighbours of *bcc* lattice. The magnitude intensity of the second peak near 0.37 nm is sensitive to the coordination number as well as geometry of third neighbours. The peak around 0.47 nm contains contributions from fourth shell and the body-diagonal sites. All of them very closely resemble the RDFs obtained from Cu K-edges for the alloy samples. Therefore, the local environment of Cu has been deduced for the three alloy samples concentrating mainly on the first peak (as appearing between 0.2 and 0.3 nm in Fig. 2(b)). For the analysis, a similar procedure as described in Refs. [18,19] has been followed, but assumed the coexistence of two kinds of neighbour for the central atom in two phases: (I) a *bcc* like Fe metallic phase and, (II) the Cu atoms on a *bcc* lattice for Cu atoms in *bcc* clusters of Cu. A good quality of fit is obtained assuming such a two site model (see Table 2). The refined values obtained from the curve fit give realistic DW factors, correct order for the bonds, an identical value of ΔE_0 for both Fe and Cu components in each alloy specimen, and a varying shift to ΔE_0 in the range of -2.2 to 6.6 eV. This later value is comparable to that of the corresponding ΔE_0 (=7.16 eV) obtained for Fe–Fe correlation from the Fe–Cu sample (Fig. 1). Therefore, the ΔE_0 parameter was allowed to vary during the fitting procedure. This

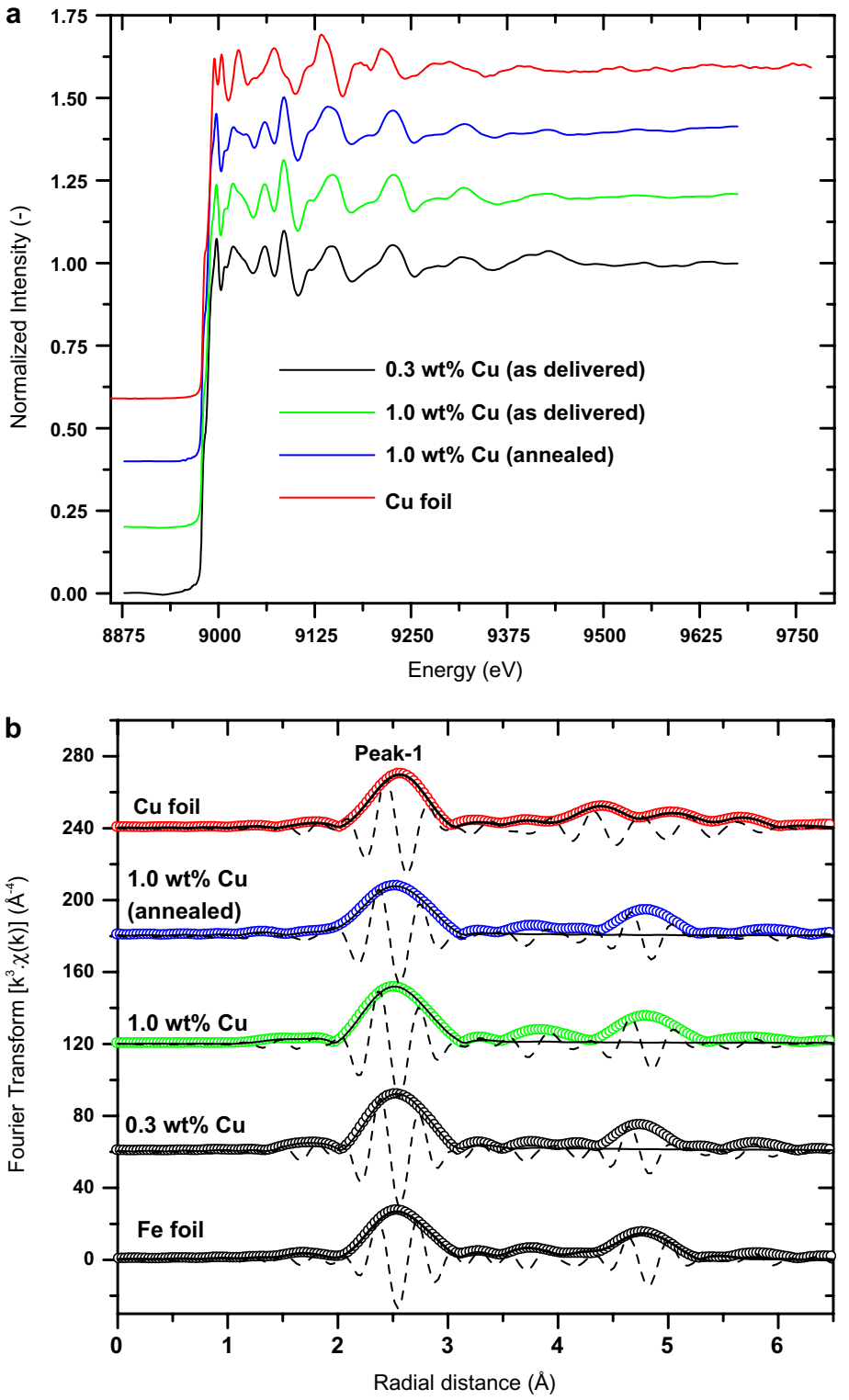

Fig. 2. (a) Normalized XAS data at 300 K in the region of the K absorption edges for pure Cu metal and three Fe–Cu binary model alloys. (b) Magnitude of the associated Fourier transforms of the experimental EXAFS data. Dot line: data; dash line: imaginary part of the transform; continuous thick line: fit. All the curves in this figure are vertically shifted with respect to each other for clarity. See the text for details.

Table 2
First-shell Cu K-edge EXAFS fit parameters for various Fe–Cu specimens

Sample	Scattering configuration	Coordination number in the first shell (–) (±10.0%)	Distance R_{NN} (nm) (±0.002)	σ^2 ($\times 10^{-4}$) (Å^2) (±5)	ΔE_0 (eV)	Quality factor $\Re$
Fe-foil	Fe–Fe	8.1	0.249	43	−2.7	0.0081
Fe–0.3 wt%Cu	Cu–Fe	8.0	0.249	51	−1.9	0.0085
	Cu–Fe	7.4	0.248	49	4.7	0.0037[a]
	Cu–Cu	0.8	0.248	49	4.7	
Fe–1.0 wt%Cu	Cu–Fe	8.0	0.248	51	−1.9	0.0126
	Cu–Fe	6.9	0.247	50	6.6	0.0034[a]
	Cu–Cu	1.1	0.249	50	6.6	
Fe–1.0 wt%Cu (annealed at 775 K)	Cu–Fe	8.0	0.248	51	−1.4	0.0176
	Cu–Fe	6.7	0.247	50	−2.2	0.0049[a]
	Cu–Cu	1.4	0.249	50	−2.2	
Cu-foil	Cu–Cu	12.2	0.253	74	4.8	0.0035

Results for the metallic Fe and Cu foils are also included. Typical error values are also mentioned.
[a] Value obtained for the two site model. See the text for details.

choice is not expected to degrade the quality of the presented results in Fig. 2.

With the assumption that only an homogeneous solid solution has been formed, the data has been also analyzed taking into account only the Cu–Fe correlation. However, as can be seen from Table 2, the two site model results a somewhat better result at the expanse of other fitting parameters and the $\Re$-factor is *lower*. Although the differences in optimized structural parameters obtained for this two cases are not large, however, it appears that the contribution from Cu–Cu correlation in peak-1 (see Fig. 2(b)) may not be negligible. Therefore, the possibility of the formation of a few atom Cu clusters (at the expense of monomers), possibly in the form of dimers, trimers or higher multimers is not ruled out in the samples that have been investigated. In this context it should be mentioned that effective phase shift calculated for *bcc* Fe is very close to that of *bcc* Cu. In addition, for the Fe–Cu samples the analysis of FT data has been performed by excluding the third- and higher-shell contributions to the Cu K-edge EXAFS spectra. Multiple-scattering effects are also not considered in the analysis. Therefore, our interpretation on the clustering of Cu atoms as against atomic populations may not be considered as definitive evidence, rather as an indicative result, at least for the Fe–0.3 wt%Cu specimen. The results presented in Table 2 indicate that for the Fe–0.3 wt%Cu specimen the $\Re$-factor is 2.2 times higher in the case of fits with Cu–Fe configuration as compared to the two-site model analysis. The corresponding change for Fe–1.0 wt%Cu specimens are about 3.7.

As already mentioned earlier that for Fe–Cu alloys containing more than 1.0 wt% Cu, the removed copper atoms from supersaturated solid solution are expected to form copper clusters or copper precipitates in the matrix. In an earlier work, Schmauder and Binkele [25] have calculated the mean size as well as size distributions of Cu precipitates in the temperature range of 673–973 K in Fe–Cu binary alloy system (having 1% copper) employing atomistic Monte Carlo simulation method. It has been shown that at 973 K precipitates of radii between 1.1 and 1.7 nm are formed within seconds in the matrix. When the temperature is decreased to 673 K, a part of the dissolved Cu atoms produces many small new precipitates and another part increases the cluster size which have formed at 973 K. According to the Fe–Cu phase diagram, at a temperature of 1075 K (used for the sample preparation in the present study) the solubility limit of Cu in Fe is about 1.2 at.%. This value is above the amount of Cu in our samples. Nevertheless, comparing our results for the 1.0 wt%Cu specimens with the results in Ref. [25] it appears that sub-nanometer size Cu clusters are formed, probably due to the nonvanishing Cu mobility at this temperature. In a previous work Deschamps et al. [26] performed TEM and small-angle X-ray scattering measurements to investigate precipitation kinetics and strengthening of a Fe–0.8 wt%Cu alloy. In their study the authors found no measurable precipitation in as-prepared samples or specimens annealed at 773 K for durations less than 5 h. This result is not in good agreement with our results, perhaps due to a slightly different sample's preparation

Table 3
Measured threshold energy (E_0) obtained from the first inflection point of the XANES data

Sample	Element	
	Cu E_0 (eV)	Fe E_0 (eV)
Fe–Cu (0.3 wt%) as prepared	8980.12 ± 0.02	–
Fe–Cu (1.0 wt%) as prepared	8979.82 ± 0.04	7111.93 ± 0.04
Fe–Cu (1.0 wt%) and annealed at 775 K	8979.85 ± 0.03	–
Cu metal foil	8979.00 ± 0.03	–
Reference K-edge energy	8979.00[a]	7111.99[a]

The error values mentioned represent the values at the peak centroid position, estimated from the best fit of the first derivative of the XANES data with a Gaussian distribution function. The energy resolution of the monochromator $(\Delta E/E) \sim 2 \times 10^{-4}$.
[a] The value is taken from http://www.csrri.iit.edu/periodic-table.html.

conditions used in this study, and/or that the limitations in the used analytical experimental technique involved in Ref. [26].

Continuing the discussion on the identification of tiny Cu clusters, let us also compare the near-edge region of the XAS spectra. A XANES comparison of all samples reveals that the Cu K-edge absorption onset energy (as determined from the inflection point) is higher in the case of Fe–Cu specimens as compared to that of metallic Cu standard, and is shifted towards higher energies. The analyzed results are shown in Table 3. The shift is small but measurable. Quantitatively, its value is nearly the same for both 1.0 wt% Cu samples and maximum (about 1.1 eV) in the case of Fe–0.3 wt%Cu specimen. The origin of this feature is still not clear. It is not straightforward to associate this difference to changes in occupancies of local electronic density of states close to the Fermi level and/or the hybridization between the 3d and 4s states in the Cu–Cu cluster bonding states [27,28]. A detail XANES analysis of the data is required considering the geometry of *bcc* Cu and becomes a subject of future investigation.

4. Summary and conclusions

In summary, XAS measurements have been carried out onto Fe–0.3 wt%Cu and Fe–1.0 wt%Cu binary model alloys. The thermal ageing effect was studied on an Fe–1.0 wt%Cu specimen annealed at 775 K for 1 h. Summing multiple files and adding adjacent points to improve the signal-to-noise ratio was an important step of the data analysis sequence. The near-neighbour atomic environment of Fe and Cu was examined by fitting the nearest-neighbour peak region of the Fourier-transformed Fe and Cu EXAFS data. Fitting of the experimental data was performed with parameterized theoretical EXAFS data generated using FEFF code. In the case of Fe K-edge data obtained from the alloy specimens they were analyzed assuming the *bcc* Fe lattice structure. The best-fit simulation for the Cu K-edge data consisted of two kinds of neighbour for the central atom, both Cu–Fe and Cu–Cu correlations, without any consideration of multiple-scattering contributions to EXAFS. Simulations have also been performed to fit the data taking into account only the Cu–Fe correlation for a comparison. The results show that both Fe and Cu atoms reside in a close-packed arrangement similar to that of *bcc* Fe. The two site model for Cu atoms provides a somewhat better description of the data. Although the differences of the optimized structural parameters obtained in the two cases are not large, however, it appears that the contribution from Cu–Cu correlation in the EXAFS data may not be negligible. Therefore, the possibility of the formation of a few atom Cu clusters, perhaps in the form of dimers, trimers or higher multimers may not be ruled out.

Acknowledgements

Thanks are due to A. Almazouzi (from Mol Belgium) for providing the samples. Acknowledgements are also due to G. Bart, D. Gavillet, A. Scheidegger (from NES, PSI), K. Dardenne and M.A. Denecke (from FZK, Germany) for their support to carry out this work. Swiss Nuclear for its financial support to LWV is also acknowledged.

References

[1] G.R. Odette, G.E. Lucas, J. Miner. Met. Mater. Soc. 53 (2001) 18.

[2] K. Fukuya, K. Ohno, H. Nakata, S. Dumbill, J.M. Hyde, J. Nucl. Mater. 312 (2003) 163.
[3] P. Asoka-Kumar, B.D. Wirth, P.A. Sterne, R.H. Howell, Philos. Mag. Lett. 82 (2002) 609, and references therein.
[4] E.F. Kneller, J. Appl. Phys. 35 (1964) 2210.
[5] J. Eckert, J.C. Holzer, W.L. Johnson, J. Appl. Phys. 73 (1993) 131.
[6] W.J. Phythian, S. Dumbill, P. Brown, R. Sinclair, in: Proceedings of the Sixth International Symposium on Environmental Degradation in Nuclear Power Systems – Water reactors, TMS, 1993, p. 729.
[7] M. Ludwig, D. Farkas, D. Pedraza, S. Schmauder, Model. Simul. Mater. Sci. Eng. 6 (1998) 19.
[8] J.Z. Liu, A. van de Walle, G. Ghosh, M. Asta, Phys. Rev. B 72 (2005) 144109, and references therein.
[9] R. Monzen, K. Takada, K. Matsuda, Z. Metallkd. 94 (2003) 1241.
[10] E.A. Kuleshova, B.A. Gurovich, Ya I. Shtrombakh, D. Yu. Erak, O.V. Lavrenchuk, J. Nucl. Mater. 300 (2002) 127.
[11] M.K. Miller, K.F. Russell, P. Pareige, M.J. Starink, R.C. Thomson, Mater. Sci. Eng. A 250 (1998) 49.
[12] D. Blavette, F. Vurpillot, P. Pareige, A. Menand, Ultramicroscopy 89 (2001) 145.
[13] S. Wei, W. Yan, J. Fan, Y. Li, W. Liu, J. Synchrotron Radiat. 8 (2001) 770.
[14] G. Salje, M. Feller-Kniepmeier, J. Appl. Phys. 48 (1977) 1833.
[15] P. Pareige, B. Radiguet, A. Barbu, J. Nucl. Mater. 352 (2006) 75.
[16] A.R. Yavari, P.J. Desre, T. Benameur, Phys. Rev. Lett. 68 (1992) 2235.
[17] See for example P.J. Schilling, J.-H. He, J. Cheng, E. Ma, Appl. Phys. Lett. 68 (1996) 767;
Y.Z. Yang, Y.L. Zhu, Q.S. Li, X.M. Ma, Y.D. Dong, G.M. Wang, S.Q. Wei, F.X. Liu, Y.Z. Chuang, Physica B 233 (1997) 119.
[18] A.B. Edwards, K.J. Roberts, S. Pizzini, W.J. Phythian, Philos. Mag. A 79 (1999) 1295.
[19] F. Maury, N. Lorenzelli, M.H. Mathon, C.H. de Novion, P. Lagarde, J. Phys.: Condens. Matter 6 (1994) 569.
[20] http://cars9.uchicago.edu/ifeffit/feffit.html.
[21] P.A. Lee, P.H. Citrin, P. Eisenberger, B.M. Kincaid, Rev. Mod. Phys. 53 (1981) 769.
[22] J.J. Rehr, J.M.D. Leon, S.I. Zabinsky, R.C. Albers, J. Am. Chem. Soc. 113 (1991) 5135, we have used the version 8.2.
[23] V.L. Moruzzi, J.F. Janak, A.R. Williams, Calculated Electronic Properties of Metals, Pergamon, New York, 1978.
[24] V.G. Harris, K.M. Kemner, B.N. Das, N.C. Koon, A.E. Ehrlich, J.P. Kirkland, J.C. Woicik, P. Crespo, A. Hernando, A.G. Escorial, Phys. Rev. B 54 (1996) 6929.
[25] S. Schmauder, P. Binkele, Comput. Mater. Sci. 24 (2002) 42.
[26] A. Deschamps, M. Militzer, W.J. Poole, ISIJ Int. (Japan) 41 (2001) 196.
[27] P.A. Montano, G.K. Shenoy, E.E. Alp, Phys. Rev. Lett. 56 (1986) 2076.
[28] K.A. Jackson, Phys. Rev. B 47 (1993) 9715.